THE JOURNAL OF PHYSICAL CHEMISTRY B

ARTICLE

pubs.acs.org/JPCB

NMR-NOE and MD Simulation Study on Phospholipid Membranes: Dependence on Membrane Diameter and Multiple Time Scale Dynamics

Megumi Shintani,[†] Ken Yoshida,[‡] Shun Sakuraba,[†] Masaru Nakahara,[†] and Nobuyuki Matubayasi[*,†,§]

[†]Institute for Chemical Research, Kyoto University, Uji, Kyoto 611-0011, Japan

[‡]Department of Chemical Science and Technology, Faculty of Engineering, University of Tokushima, 2-1 minamijosanjima-cho, Tokushima 770-8506, Japan

[§]Japan Science and Technology Agency (JST), CREST, Kawaguchi, Saitama 332-0012, Japan

ABSTRACT: Motional correlation times between the hydrophilic and hydrophobic terminal groups in lipid membranes are studied over a wide range of curvatures using the solution-state ^{1}H NMR-nuclear Overhauser effect (NOE) and molecular dynamics (MD) simulation. To enable ^{1}H NMR-NOE measurements for large vesicles, the transient NOE method is combined with the spin−echo method, and is successfully applied to a micelle of 1-palmitoyl-lysophosphatidylcholine (PaLPC) with diameter of 5 nm and to vesicles of dipalmitoylphosphatidylcholine (DPPC) with diameters ranging from 30 to 800 nm. It is found that the NOE intensity increases with the diameter up to ∼100 nm, and the model membrane is considered planar on the molecular level beyond ∼100 nm. While the NOE between the hydrophilic terminal and hydrophobic terminal methyl groups is absent for the micelle, its intensity is comparable to that for the neighboring group for vesicles with larger diameters. The origin of NOE signals between distant sites is analyzed by MD simulations of PaLPC micelles and DPPC planar bilayers. The slow relaxation is shown to yield an observable NOE signal even for the hydrophilic and hydrophobic terminal sites. Since the information on distance and dynamics cannot be separated in the experimental NOE alone, the correlation time in large vesicles is determined by combining the experimental NOE intensity and MD-based distance distribution. For large vesicles, the correlation time is found to vary by 2 orders of magnitude over the proton sites. This study shows that NOE provides dynamic information on large vesicles when combined with MD, which provides structural information.

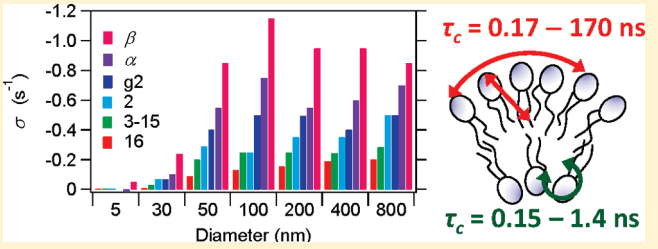

1. INTRODUCTION

A bilayer membrane is composed of amphiphilic lipids facing their hydrophilic headgroups toward the outer water pools and their hydrocarbon tails toward the inner hydrophobic core region. The intermolecular interactions between the lipid components play a key role in controlling the functions of the biological membranes. The permeabilities of smaller molecules have been found to be tuned by the interactions between hydrophobic tail groups,[1−16] and the formation of the raft domain has been investigated in relation to the interactions between hydrophilic headgroups.[17−19] Toward the full understanding of the phenomena at the molecular level, the dynamic interactions between the hydrophilic and hydrophobic portions are of great importance.

In the present study, we shed light on the effect of membrane curvature on lipid dynamics. The intermolecular forces between neighboring lipid molecules are sensitive to the membrane curvature, since it determines the average distance between the atomic sites of neighboring lipids. When the membrane curvature is large, the inner side of the vesicle is more highly packed and the outer side is less. The change in the phase transition temperature is the most well-known manifestation of the curvature effect.[20−24] The relation of curvature effect to biological functions has attracted great attention since it is considered to regulate biological functions such as binding of proteins and drugs, membrane fusion and division, and domain formation.[25−31] The lipid dynamics plays essential roles in these functions, and the curvature effect on the dynamics needs to be elucidated at atomic resolution.

For the studies on the dynamic phenomena associated with the membrane curvature, nuclear Overhauser effect (NOE) measurement of the NMR spectroscopy is a powerful experimental method that provides us with the intermolecular distance and the correlation time at the atomic level.[16,18,32−39] NOE studies on membranes are few in number, however, because of severe signal broadenings, especially for a membrane with small curvature in an aqueous phase.[40] In this study, we propose a new solution-state ^{1}H NMR sequence for the NOE measurement with a spin−echo part to minimize undesirable and unavoidable broad components of membrane NMR spectra. Deuteration of

Received: May 2, 2011
Revised: June 20, 2011
Published: July 05, 2011

the lipid alkyl chains, which was adopted in our previous study,[18] is not applicable in the present study, since the alkyl chains are the atomic sites of focus. Furthermore, the variation of curvature with vesicle diameter requires very high water content in the sample solution, which is not suitable for the solid-state NMR. In this study, we demonstrate the validity and the effectiveness of the newly proposed pulse sequence over a wide range of curvature.

In order to obtain a realistic molecular picture from the NOE measurement, it is often necessary to take advantage of a dynamic model or a computational method such as molecular dynamics (MD) simulation.[35,41−47] The widely used conventional approaches to avoid the parallel use of such models or calculations are the fixed-correlation-time and the fixed-distance approximations. The former one is often applied for the structure determination, and the latter is for the flexibility of each portion of macromolecules, and both of them can be safely applied for proteins in most cases.[32,48−50] In the case of fluids, however, the separation of the contributions from the distance and the correlation time is not straightforward since the diffusion process affects both the distance and the correlation time.[43,45,47] In lipid bilayers, the examination of the origin of NOE is more complicated owing to the dynamic modes specific to membranes, such as lateral diffusion, fluctuation in the vertical direction, rotation around the long axis of the lipid molecule, undulation, overall tumbling, and flip-flop.[10,37,51−55]

To resolve the origin of the NOE into the contributions of the distance and the correlation time, the MD simulation is advantageous. Although the internuclear distance and the correlation time cannot be separated with the NOE experiment alone, they can be separately treated with MD. Indeed, Gawrisch, Feller, and co-workers employed the solid-state NMR and MD in complementary manner and examined the origin of membrane NOE including the effects of lateral diffusion and spin diffusion.[16,33,34,36,37,44,46] To obtain MD data that can be well combined with experimental NOE, we conduct MD simulation on micelles and planar bilayers as the extremes of large and small curvatures, and obtain the distance distribution and the correlation function. The MD analysis is combined with the NOE measurement to elucidate the dependence of the correlation time on the proton pair. By utilizing the combination of NMR-NOE experiment and MD simulation, we discuss the curvature effect on the dynamics of lipid membrane in the solution state. In fact, our analysis of NOE is based only on the statistical-mechanical expression for NOE and does not use specific properties of the membrane. It could thus have an impact on other systems such as transmembrane proteins and ionic liquids.

The organization of this paper is as follows. The experimental part is in section 2. In subsection 2.1, the materials and the sample preparations are explained. In subsection 2.2, the NMR measurement conditions are described and the new NOE method is presented. In subsection 2.3, the theoretical expression for the NOE is given. In subsection 2.4, the MD setups are described. Results are presented and discussed in section 3. In subsection 3.1, our NOE method is compared with the conventional method. In subsection 3.2, the curvature dependence of the NOEs is shown. In subsection 3.3, the internuclear distance obtained from MD simulation is described. In subsection 3.4, the correlation time is discussed by combining NOE and MD results. Conclusions are given in section 4.

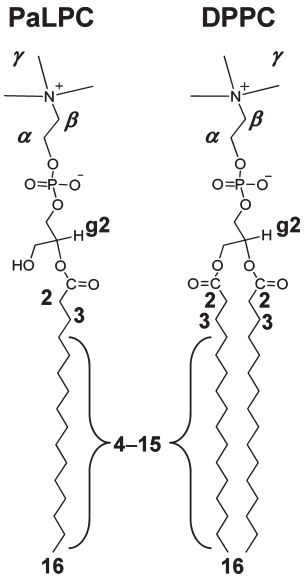

Figure 1. The molecular structures of PaLPC and DPPC.

2. METHODS

2.1. Materials and Sample Preparations. Micelles and vesicles were formed by 1-palmitoyllysophosphatidylcholine (PaLPC) and dipalmitoylphosphatidylcholine (DPPC), respectively. PaLPC and DPPC with a purity of 99% were purchased from Wako Pure Chemical Industries and Sigma (St. Louis, USA), respectively. See Figure 1 for the molecular structures and the proton numbering. Chloroform (99%) and methanol (99.8%) used for the vesicle preparation were supplied by Nacalai. Heavy water (D_2O; 99.9% D) was from Euriso-top (Saint Aubin, France).

The micellar solution was prepared from PaLPC and D_2O (20 mM). The small unilamellar vesicle (SUV) of DPPC was prepared by ultrasonic irradiation of aqueous suspension of DPPC with MISONIX MICROSON Model XL2000 at an amplitude of 45 μm for 20 min. The average diameter was 5 and 30 nm for the PaLPC micelle and DPPC SUV, respectively.[25,51,56] The aqueous suspensions of large unilamellar vesicles (LUVs) were prepared as follows. DPPC 73.4 mg was dissolved in $CHCl_3$ 5 mL, and evaporated overnight in a high vacuum to form a thin lipid film using a rotary evaporator (Iwaki) at 50 °C. A thin lipid film was fully hydrated with an appropriate volume of D_2O to yield a final concentration of 20 mM for DPPC. This aqueous suspension was then subjected to freeze−thaw method over eight cycles using hot water bath of 60 °C and liquid nitrogen. The LUVs were extruded at 60 °C for more than 31 passes through a polycarbonate filter (Nuclepore Track-Etch Membrane, Whatman Schleicher & Schuell) with pore diameters of 50, 100, 200, 400, and 800 nm. We used Mini-Extruder (Avanti Polar Lipids, Inc.) and EXTRUDER (Lipex Biomembranes, Inc.).[57,58] The extrusion by utilizing EXTRUDER was performed by N_2 gas of ∼1 MPa.[59]

2.2. NMR Measurement: Transient NOE-SE Method and Practice. NMR measurements were performed by using a JEOL ECA600 NMR spectrometer with a specially designed diffusion probe HX5GR.[12] The ^{1}H frequency was 600 MHz. The suspended model membranes were measured at 60 °C, which is above the gel−liquid crystal phase transition temperature of

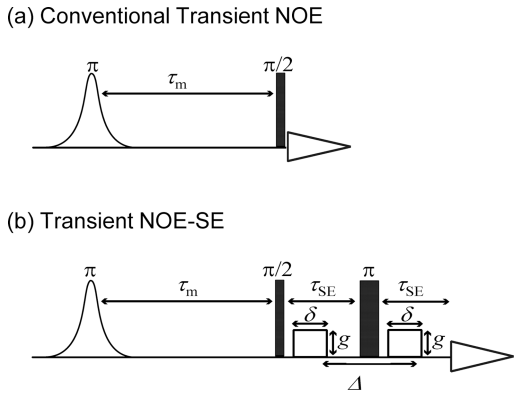

Figure 2. The pulse sequences of (a) the conventional transient NOE and (b) the transient NOE-SE.

DPPC (37−42 °C: it depends on the diameter of the vesicle[20−24]). The impurity HDO signal contained in solvent D_2O was used as the internal reference for the chemical shift.[60]

The conventional transient NOE method was combined with the spin−echo (SE) method (we call it the transient NOE-SE method). The broad signals are suppressed by the spin−echo part of the transient NOE-SE sequence and the sharp signals are detected against apparently flat baseline. The pulse sequences of the conventional transient NOE and the transient NOE-SE are shown in Figure 2. The conventional transient NOE sequence is given by $\pi-\tau_m-\pi/2$, where τ_m is the mixing time. The transient NOE-SE sequence supplements the conventional transient NOE with the spin−echo sequence $\pi/2-\tau_{SE}-\pi-\tau_{SE}$, where τ_{SE} is the delay time, and reads as $\pi-\tau_m-\pi/2-\tau_{SE}-\pi-\tau_{SE}$. Broad signals that have spin−spin relaxation times (T_2) much smaller than τ_{SE} are suppressed within the spin−echo period. Sharp signals with $T_2 \gg \tau_{SE}$ are refocused without appreciable intensity loss. The broad components vanish apparently into the baseline; the sharp components are well resolved, and their NOE can be determined quantitatively. High-quality NOE signals can also be obtained by using such sophisticated schemes as the gradient enhanced NOE (GOESY)[61] and the double-pulsed-field-gradient spin−echo (DPFGSE) NOE.[62] Our NOE scheme developed here is simpler and still enables the quantitative assessment of the cross relaxation rate, as shown in subsection 3.1. To the best of our knowledge, there are no NOE studies on lipid bilayer membranes to suppress their broad signals by the spin−echo scheme.

HDO is contained in D_2O as an impurity, and its peak intensity is still much stronger than the intensities of the target peaks. To suppress the HDO signal, the pulse-field gradient is used during the spin−echo delay period as shown in Figure 2b. The use of the pulse-field gradient exploits the fact that the self-diffusion coefficient of HDO is much larger than that of phospholipids composing bilayer membranes. The signal intensity I after the application of a pulse-field gradient is given by

$$I = I_0 \exp\left(-\gamma^2 D\delta^2\left(\frac{4\Delta-\delta}{\pi}\right)g^2\right) \quad (1)$$

where I_0 is the signal intensity without the pulse-field gradient, γ is the gyromagnetic ratio of the observed nucleus, D is the self-diffusion coefficient, δ and Δ are the width of the two gradient pulses and the time interval between them, respectively, and g is the strength of the applied gradient.[63] A signal intensity declines exponentially with the self-diffusion coefficient D. Here, the systems consist only of water and phospholipids, and only the HDO signal with much larger D is affected by appropriate choices of δ, Δ, and g. In this study, δ = 0.8−1.4 ms (differs by the HDO content in the sample), Δ = 3 ms, and g = 1.5 Tm^{-1} were adopted, and the HDO signal was found to decline to the level of the choline signals from phospholipids. It should be noted that the field gradient is not the essential part of the transient NOE-SE method. The gradient is used only to suppress the water signal.

The NOE enhancement factor η at a mixing time τ_m is related to the cross relaxation rate constant σ by an initial rate approximation[50]

$$\eta(\tau_m) = 2\sigma\tau_m \quad (2)$$

when τ_m is small enough. In practice, η is determined from

$$\eta(\tau_m) = \frac{I(\tau_m) - I_{SE}}{I_{SE}} \quad (3)$$

where I_{SE} is the integrated intensity of the reference spectrum from the spin−echo signal without NOE and $I(\tau_m)$ is the integrated intensity in the sample spectrum modified by the NOE.

2.3. Theoretical Expressions for NOE Cross Relaxation Rate Constant. The nuclear magnetic relaxation for protons is mainly caused by the dipole−dipole interaction. The time correlation function $C(t)$ for the dipole−dipole interaction is expressed as

$$C(t) = \xi\langle r(0)^{-3} r(t)^{-3} Y_2^0(\Omega(0)) Y_2^0(\Omega(t))\rangle \quad (4)$$

where t is the time, ξ is a constant given below, $Y_2^0 = (3\cos^2\theta - 1)/2$ is the normalized second-order spherical harmonics, and $\Omega(t) = \{\theta(t), \varphi(t)\}$ is the set of polar angles in the laboratory reference frame for the unit vector connecting the two protons of interest.[43,50,64,65] The angular bracket means the ensemble average over the equivalent proton pairs and over the orientation of the dipole−dipole unit vector relative to the laboratory reference frame. The constant ξ is given by

$$\xi = \frac{3\mu_0^2\hbar^2\gamma^4}{8\pi^2} \quad (5)$$

where μ_0 is the permeability of vacuum, $\hbar$ is the Planck constant divided by 2π, and the γ is the gyromagnetic ratio of proton. When the system of interest is macroscopically an isotropic fluid, eq 4 can be averaged over the uniform distribution of the magnetic-field orientation and reduces to

$$\begin{aligned} C(t) &= \xi\langle\langle r(0)^{-3} r(t)^{-3} P_2(\overrightarrow{n(0)}\cdot\vec{H}) P_2(\overrightarrow{n(t)}\cdot\vec{H})\rangle_{\vec{H}}\rangle_{pr} \\ &= \frac{1}{5}\xi\langle r(0)^{-3} r(t)^{-3} P_2(\overrightarrow{n(0)}\cdot\overrightarrow{n(t)})\rangle_{pr} \end{aligned} \quad (6)$$

In eq 6, $\langle\ldots\rangle_{pr}$ is the ensemble average over the proton pairs, $\vec{H}$ is the orientation of the magnetic field, $\langle\ldots\rangle_{\vec{H}}$ is the average over the uniform distribution of the magnetic-field orientation. The r and $\vec{n}$ denote the radial distance between the proton pair of interest and the unit vector connecting them, respectively, and P_2 is the second Legendre polynomial. In the following, we redefine $\langle\ldots\rangle = \langle\ldots\rangle_{pr}$ for notational simplicity. $C(t)$ is expressed as a sum of the contributions from the observed protons of type a and the irradiated protons of type b and is

given by

$$C(t) = \frac{1}{N_a}\sum_a\sum_b C_{ab}(t) \quad (7)$$

where N_a is the number of observed protons of type a. It should be noted that eq 7 involves intra- and intermolecular contributions. These two contributions may exhibit different time profiles. The correlation time τ_c is defined as

$$\tau_c = \int_0^\infty \frac{C(t)}{C(0)}\,dt \quad (8)$$

where

$$C(0) = \frac{1}{5}\xi\langle r^{-6}\rangle \quad (9)$$

$\langle r^{-6}\rangle$ is given by

$$\langle r^{-6}\rangle = \int \rho(r) r^{-6}\,dr \quad (10)$$

and

$$\rho(r) = \frac{1}{N_a}\sum_a\sum_b \langle\delta(r_{ab} - r)\rangle \quad (11)$$

The spectral density $j(\omega)$ is the Fourier transform of $C(t)$ and provides the cross relaxation rate constant σ for a homonuclear spin system through

$$\sigma = \frac{1}{24}\{6j(2\omega_0) - j(0)\} \quad (12)$$

where ω_0 is the Larmor frequency in angular units. When the resonance frequency is 600 MHz, $1/\omega_0$ = 0.27 ns. When $C(t)$ relaxes much faster than $1/\omega_0$ (motional narrowing limit; $1/\omega_0 \gg \tau_c$), $j(2\omega_0)$ is virtually identical to $j(0)$ and

$$\sigma = \frac{5}{24}j(0) = \frac{5}{12}C(0)\tau_c \quad (13)$$

since $j(0) = 2C(0)\tau_c$. When $C(t)$ relaxes much slower than $1/\omega_0$ ($1/\omega_0 \ll \tau_c$), $j(2\omega_0)$ is negligibly small and

$$\sigma = -\frac{1}{24}j(0) = -\frac{1}{12}C(0)\tau_c \quad (14)$$

In fact, the σ in large vesicles can be approximated by eq 14 according to the results in subsection 3.4. When $C(t)$ is expressed as a sum of exponential functions through

$$C(t) = \frac{1}{5}\xi\langle r^{-6}\rangle\sum_n A_n \exp\left(-\frac{t}{\tau_n}\right) \quad (15)$$

with $\Sigma_n A_n = 1$, the spectral density function is given by

$$j(\omega) = \frac{2}{5}\xi\langle r^{-6}\rangle\sum_n \frac{A_n\tau_n}{1 + \omega^2\tau_n^2} \quad (16)$$

and the cross relaxation rate constant σ is correspondingly written as

$$\sigma = \frac{\mu_0^2\hbar^2\gamma^4}{160\pi^2}\langle r^{-6}\rangle\left(6\sum_n \frac{A_n\tau_n}{1 + 4\omega_0^2\tau_n^2} - \sum_n A_n\tau_n\right) \quad (17)$$

2.4. MD Simulation. MD simulation was performed in water for the PaLPC micelle and DPPC planar bilayer. The aggregation number of the PaLPC micelle was set to 139.[66] In the MD unit cells for the micelle and bilayer systems, 139 PaLPC with 29955 water molecules and 458 DPPC with 34504 water molecules were located, respectively. The total number of atoms in the unit cell is 163052 and 101402 for the PaLPC and DPPC systems, respectively. The all-atom CHARMM force field PARAM27R was used for the lipid,[67−70] and the TIP3P model was adopted for the water molecule.[71] The periodic boundary condition was employed, and the unit cell was taken to be rectangular. The ensemble adopted was the *NPT* (constant particle numbers, pressure, and temperature) for the PaLPC micelle and the NP_nAT (constant particle numbers, normal pressure, lateral area, and temperature) for the DPPC planar bilayer. The pressure and temperature were controlled at 1 bar and 60 °C, respectively, with the Nosé−Hoover Langevin method at time constants of 5.0 ps^{-1}.[72,73] The lateral area of the unit cell of the DPPC system was set to 64 $Å^2$ in the square form.[74] The electrostatic interaction was handled by the particle-mesh Ewald (PME) method with a real-space cutoff of 9.5 Å, a spline order of 6, and a relative tolerance of 10^{-5}. The reciprocal-space mesh size was 108 × 108 × 108 and 120 × 120 × 128 for the PaLPC and DPPC systems, respectively. The Lennard-Jones interaction was truncated by applying the switching function, where the switching range is 8.5−9.5 Å. The bond lengths involving the hydrogen atom were fixed with SHAKE, and the water molecule was kept rigid with SETTLE.[75] The equation of motion was integrated with the velocity Verlet algorithm at a time step of 2 fs.[76] All the MD calculations were done for 20 ns using NAMD ver.2.7b2.[77]

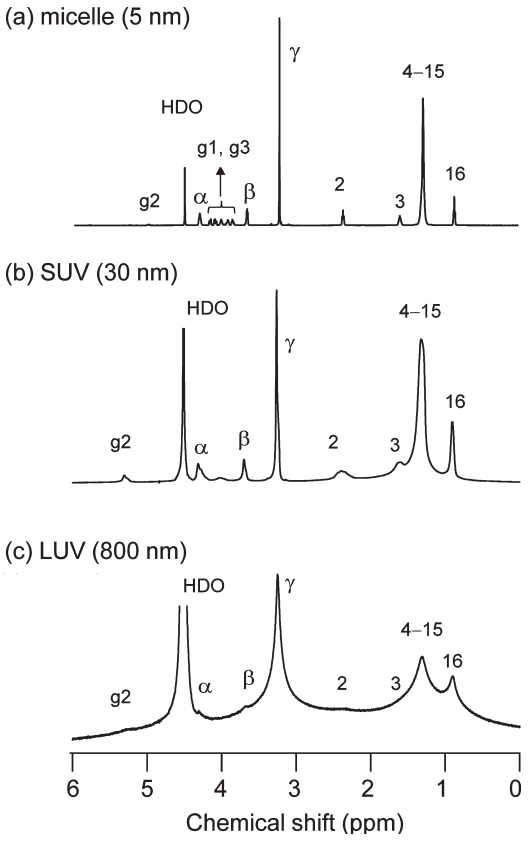

Figure 3. ^{1}H NMR spectra of a micelle, SUV, and LUV 800 nm in diameter.

3. RESULTS AND DISCUSSION

In subsection 3.1, we show the performance of the transient NOE-SE method described in subsection 2.2. In subsection 3.2, we describe the curvature dependence of the NOE signals obtained by the transient NOE-SE method. In subsection 3.3, we analyze the MD results on atomic distances in model membranes in connection to the cross relaxation rate. In subsection 3.4, we combine the NOE and MD analysis and discuss the site dependence of the correlation time. In the following, the proton sites attached to the choline methyl group and the hydrophobic terminal methyl group are denoted, respectively, as PCγ or PC16, for example, by using the character or number shown in Figure 1. A correlated pair of proton sites is indicated by using a slash, for example, PCγ/PCβ for denoting the correlation between the PCγ and PCβ sites.

3.1. Comparison of Conventional Transient NOE and Transient NOE-SE. We first demonstrate the low resolution of the ^{1}H signals in LUVs. Figure 3 shows the solution-state ^{1}H NMR spectra of (a) a PaLPC micelle (5 nm in diameter), (b) a DPPC SUV (30 nm), and (c) a DPPC LUV (800 nm). Evidently, the line width of smaller model membrane is sharper than that of larger. All the signals of the micelle are clearly separated. The primary reason why a micelle is well employed in solution ^{1}H NMR studies is the high resolution of the chemical shift. Also in the case of SUVs, the signal is reasonably sharp. The advantages of NMR are thus well enjoyed for using an SUV as a model vesicle.[40] In the case of the LUV of 800 nm in diameter, only broad signals are obtained; the signal overlap is significant, and no clear baseline can be defined. Three signals are identified in Figure 3c: the terminal hydrophilic group (PCγ), the hydrophobic chain (PC3−15), and terminal methyl group (PC16). Due to the signal overlap, the quantitative approach using integrated intensities is difficult, and the NMR analysis is subject to severe limitations. Furthermore, an irradiation by selective pulse is troublesome and an NOE measurement is hardly performed.

Next we show how the transient NOE-SE method improves the NOE spectrum of LUVs. Figure 4 shows the feature of the spectra from the present transient NOE-SE method and the conventional transient NOE method applied to an LUV membrane of 400 nm in diameter. The hydrophilic headgroup (PCγ) was irradiated by the selective π pulse. PCγ is chosen for selective irradiation since we later examine the correlation between the outermost site and the other sites in the lipid molecule. For DPPC, the PCγ signal is the strongest and is well separated from the others. According to Figure 4a, the conventional transient NOE method provides broad signals, in particular, for the acyl chain (PC3−15) whose signals overlaps with that of the terminal methyl group (PC16); the signal broadening prohibits the atomic-level study of membrane structure. This limitation is overcome by the transient NOE-SE pulse sequence as can be seen from Figure 4b. The signals of PC16 and PC3−15 are well separated. The broad components in the spectrum are suppressed by the spin−echo part, and an almost flat baseline is obtained. An atomic-level analysis will now be possible, for example, for the correlation between the hydrophilic terminal (PCγ) and the hydrophobic terminal (PC16).

The effect of spin−echo is more striking when the spectrum is broader without spin−echo. To assess the reduction of the line width, we examine the ratio of the ^{1}H's full width at half height

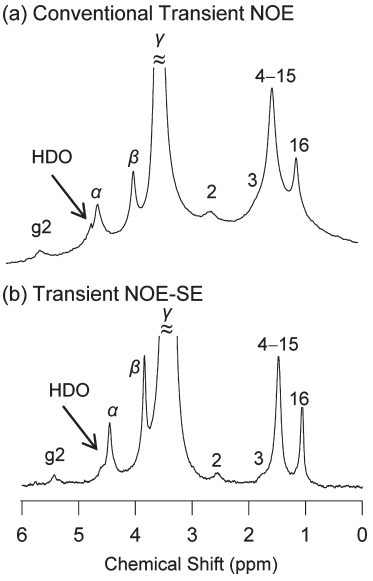

Figure 4. The transient NOE difference spectra when (a) the conventional transient NOE and (b) transient NOE-SE pulse sequence were applied to LUVs of 400 nm. The mixing time was 100 ms.

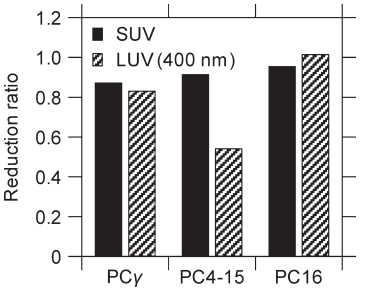

Figure 5. The fwhh reduction for SUVs and LUVs of 400 nm diameter. The reduction is expressed as the ratio of the fwhh with and without the spin−echo.

(fwhh) with and without the spin−echo. Figure 5 shows the ratio for the SUV and the LUV of 400 nm diameter. In each case, the fwhh is reduced with the spin−echo. The reduction is strongest for PC3−15 of LUV. Indeed, this peak has the largest line width without spin−echo; the peak of PC3−15 is actually a composition of the peaks from nonequivalent protons.

To further validate the transient NOE-SE method, we examine the mixing-time dependence of the NOE enhancement factor η of eq 3 in our transient NOE-SE and the conventional transient NOE methods (Figure 6). This is done for the SUV system since both of the methods provide sharp enough signals. The NOE enhancements are too small for the micelle, as shown in subsection 3.2, and they cannot be obtained in the conventional method for the LUV. In Figure 6, the two methods provide the corresponding profiles against the mixing time τ_m at each site, and the τ_m with maximum enhancement is also common. To determine the cross relaxation rate constant σ from η through eq 2, τ_m needs to be small enough to ensure the linear approximation, and at the same time, it is desirable to be large enough to have η with good S/N. To satisfy these conditions, we base our discussion on the NOE data at τ_m = 100 ms in the following.

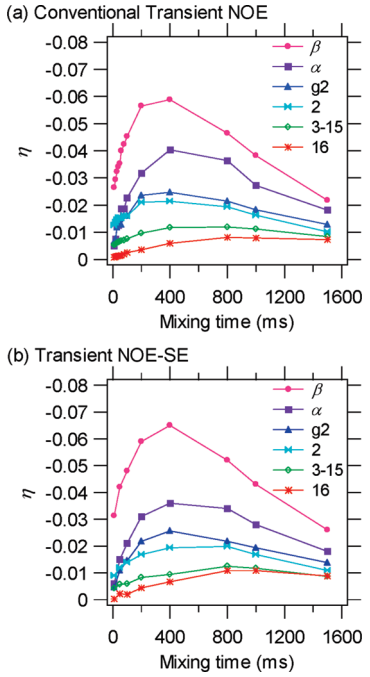

Figure 6. The mixing-time dependence of the NOE enhancements η for the SUV system (a) in the conventional transient NOE and (b) in the transient NOE-SE experiment with the selective π pulse applied to PCγ.

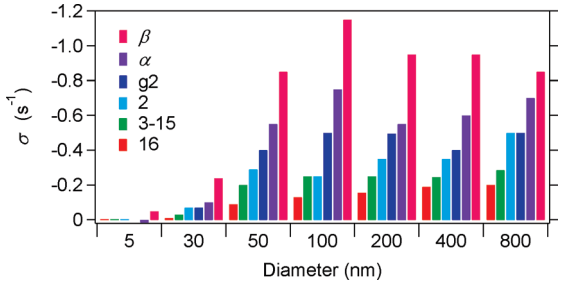

Figure 7. The vesicle size dependence of the cross relaxation rate constant σ between PCγ and the other sites. The σ values are determined from the NOE-SE enhancement factor η and the mixing time τ_m through eq 2; the NOE-SE enhancement factor $\eta(\tau_m) = \{I(\tau_m)-I_{SE}\}/I_{SE}$ was obtained by the PCγ irradiation at τ_m = 100 ms. Here $I(\tau_m)$ is the integrated intensity in the spectrum modified by the NOE and I_{SE} is the integrated intensity of the reference spectrum. This reference was taken by the spin−echo method using the same values of τ_{SE} (3 ms), δ (0.8−1.4 ms), and g (1.5 Tm^{-1}) as those for the transient NOE-SE method. The diameters of 5 and 30 nm correspond to the PaLPC micelle and the DPPC SUV vesicle, respectively.

3.2. Experimental Observation of NOE. In this subsection, we discuss the curvature dependence of the cross relaxation rate constant σ. Figure 7 shows the σ determined from the NOE-SE enhancement factor η and the mixing time τ_m through eq 2. The diameter (inverse curvature) examined ranges from 5 nm (micelle) to 800 nm (LUV). The transient NOE-SE method enables the quantitative determination of the site dependence of σ even for a LUV of 800 nm in diameter, which does not provide a well-resolved spectrum by using the conventional method. In the micelle, the σ is significantly smaller than in the vesicles. As shown in subsections 3.3 and 3.4, the small

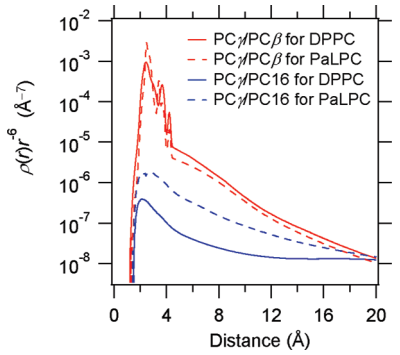

Figure 8. MD simulation results of $\rho(r)r^{-6}$ plotted against the distance r from PCγ of PaLPC (solid line) and DPPC (dashed line).

enhancement is due to a rapid, structural fluctuation of micelle.

A general observation in Figure 7 is that the σ increases in magnitude with the membrane diameter (curvature reduction) from 30 to ∼100 nm. Beyond ∼100 nm, the NOE becomes less dependent on curvature. The variation of the σ values with vesicle diameter is within ∼10%, which corresponds to the experimental uncertainties.[78] The model membrane is thus essentially planar beyond ∼100 nm in regard to the NOE measurements. As shown in subsection 3.4, the curvature dependence of σ is caused mainly by that of the correlation time τ_c, not by that of the distance r.

In Figure 7, the cross relaxation rate constant σ in the vesicles is larger in magnitude for a site closer to PCγ irradiated. The observation of the NOE in LUVs even between the hydrophilic headgroup (PCγ) and the hydrophobic terminal methyl group (PC16) is rather surprising, because the PCγ and PC16 are about 30 Å apart in the intramolecular structure.[79] In a solid-state NMR, Huster and Gawrisch also pointed out the detectability of the NOE between the most distant pairs in multilamellar vesicles.[33] They denied the possibility of spin diffusion along the hydrocarbon chains by a systematic partial deuteration of the alkyl chains. The spin diffusion is not appreciable in our results of solution-state NMR method, either, as is inferred in the mixing-time dependence of the NOE enhancement factors shown in Figure 6.[80] Thus, the large σ for PCγ/PC16 at small curvature comes from a high probability of close contact and/or a long correlation time. The quantitative analysis of the weight of the two contributions requires insights from MD, and is discussed in the following subsections 3.3 and 3.4.

3.3. Contact Distance between Atomic Sites. The cross relaxation rate constant σ is dependent on the internuclear distance r and the correlation time τ_c as described in subsection 2.3. Since it is impossible to decompose the NOE into the r and τ_c contributions by the NOE experimental results alone, we make use of MD simulation. In this subsection, we analyze the internuclear distances in terms of the distribution functions $\rho(r)$ of eq 11 introduced in subsection 2.3. The correlation time is discussed in the next subsection.

In Figure 8, we plot the quantity $\rho(r)r^{-6}$ for the PaLPC micelle and DPPC planar bilayer, since the distance contribution appears in the form of $\rho(r)r^{-6}$ in the expression of the cross relaxation rate (eq 10). The hydrophilic−hydrophilic distance distribution is examined with the PCγ and PCβ pair. Both of the PaLPC micelle and the DPPC planar bilayer show a strong peak at ∼3 Å, well below the rule-of-thumb distance of 5 Å within which a contact pair gives rise to a large NOE. The curvature dependence is negligibly small, as is seen in the almost

dx.doi.org/10.1021/jp204051f |J. Phys. Chem. B 2011, 115, 9106–9115

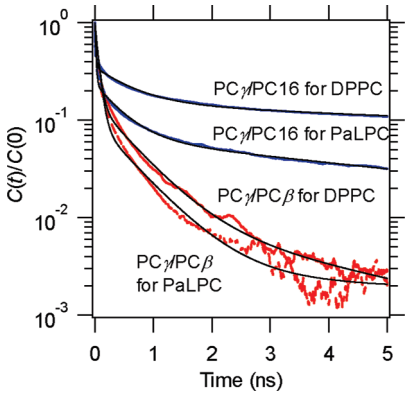

Figure 9. The normalized correlation function, $C(t)/C(0)$, of PCγ/PCβ (red) and PCγ/PC16 (blue). The plotted values are the sum of intra- and intermolecular correlations. The black lines represent the fits to the calculated $C(t)/C(0)$ by a sum of three exponential functions.

overlapping plots of $\rho(r)r^{-6}$ for the micelle and the planar bilayer. From the static viewpoint of the distance distribution, the interactions in the hydrophilic region are essentially independent of the membrane curvature.

The $\rho(r)r^{-6}$ plot for the hydrophilic−hydrophobic pair PCγ/PC16 also shows a noticeable peak at ∼3 Å. Although the peak intensities for both micelle and planar bilayer are orders-of-magnitude smaller in comparison to those for PCγ/PCβ, the peak is clear evidence of the close contact between even the most distant PCγ/PC16 pair. The PCγ/PC16 distance distribution is, unlike the PCγ/PCβ distance, clearly curvature-dependent. The $\rho(r)r^{-6}$ value for PCγ/PC16 is larger by an order of magnitude for the PaLPC micelle. The probability of PCγ/PC16 proximity is larger in the micelle than in the planar bilayer. This is presumably because the vertical fluctuation is more remarkable in micelles in which the headgroup region is less packed and the planar ordering is more difficult. It is of interest to note that the curvature dependencies of the $\rho(r)r^{-6}$ and the experimental σ are opposite in the case of PCγ/PC16, whereas the σ is proportional to the integral of $\rho(r)r^{-6}$ over r (subsection 2.3). The present experimental results in Figure 7 show that the NOEs are strongly detectable for large vesicles and are not observable in micelles except for the weakly detectable one of the PCγ/PCβ pair. Factors underneath this apparent inconsistency are quantitatively revealed in the following subsection in terms of the curvature dependence of the correlation times.

3.4. Multiple Time Scales of Motion. The correlation time τ_c is given by the decay of the time correlation functions $C(t)$ (eq 8), and a longer τ_c leads to a larger cross relaxation rate σ (eqs 13 and 14). In this subsection, we examine the time correlation function $C(t)$ that determines the NOE in combination with the distance distribution factor $\rho(r)r^{-6}$. In Figure 9, we show $C(t)$ in the PaLPC micelle and the DPPC planar bilayer. A curvature effect, observed as the difference between the micelle and planner bilayer, is noticeable for both of the PCγ/PCβ and PCγ/PC16. In both cases, $C(t)$ for the planner bilayer decays more slowly than for the micelle. Since the slower decay of $C(t)$ gives a larger τ_c and thus leads to a larger σ, the difference in $C(t)$ between the micelle and planar bilayer corresponds to the experimental results on NOE.

The curvature effect on the $C(t)$ decay for the PCγ/PC16 is significantly larger than that for PCγ/PCβ. It is interpreted in terms of lateral diffusion and tumbling motion. The angle of the intermolecular PCγ/PC16 vector is mainly changed due to the lateral diffusion in the plane of the bilayer. The tumbling motion contributes to the orientation of the intramolecular PCγ/PC16 vector. The tumbling is considered to occur in the time scale of several nanoseconds and milliseconds for the micelle and vesicle, respectively, from Stokes−Einstein−Debye law.[49] The lateral diffusion in the planar membrane is considered to be faster, but is still in the submicrosecond time scale.[34,37,44,46] The effects of the slow dynamics on the PCγ/PCβ vector will be significantly smaller than on the PCγ/PC16 vector since its orientation is changed rapidly by the rotation of methyl groups.

Table 1. Correlation Times Estimated by the $C(t)$ Fitting

	τ_c (ns)	
system	PCγ/PCβ	PCγ/PC16
PaLPC (MD fit)	0.17	0.54
DPPC (MD fit)	0.17	2.7

We next compare the $C(t)$'s of the PaLPC micelle and the DPPC planar bilayer. According to Figure 9, the difference in $C(t)$ between the micelle and the planar bilayer is small for the neighboring pair of protons PCγ/PCβ. For the distant pair PCγ/PC16, on the other hand, the $C(t)$ difference is much larger, and the decay is slower for the planar bilayer. This means a stronger curvature effect on distant pairs. A model membrane with a smaller curvature involves a stronger inhomogeneity in the dynamical time scale. For the DPPC planar bilayer, the difference in τ_c compensates for the difference in $\rho(r)r^{-6}$ and leads to a comparable σ over a wide range of distances between the proton pair.

To quantify τ_c, we adopt the fitting to a linear combination of three exponential terms, $C(t)/C(0) = \Sigma_n^3 A_n \exp(-t/\tau_n)$. Then the summed correlation time, which is useful for discussing the cross relaxation, is obtained as $\tau_c = \Sigma_n^3 A_n \tau_n$ and is listed in Table 1. In the case of the PaLPC micelle, τ_c is on the order of subnanoseconds for both PCγ/PCβ and PCγ/PC16.[81] According to the $\rho(r)r^{-6}$ and the $C(t)$ obtained from MD, the σ in the PaLPC micelle is 0.2 and -0.002 s^{-1} for PCγ/PCβ and PCγ/PC16, respectively, from eq 17. The calculated σ value for PCγ/PCβ is above the threshold of experimental detection limit of the NOE enhancement factor,[82] and that for PCγ/PC16 is an order of magnitude less than the detection limit experimentally available. This is in agreement with the experimental results for the PaLPC micelle that the σ for a close pair of protons is detectable and that σ for distant pairs is too small to be detected.

The τ_c values of the DPPC planar bilayer estimated by the $C(t)$ fitting are rough underestimates, however, due to the absence of slow components of $C(t)$ such as lateral diffusion and tumbling within the time scale of Figure 9. The examination of τ_c in relation to NOE is not as complete as that for micelles, especially with regard to the slow component of the $C(t)$ decay. Additionally, even if we perform sufficiently long-time simulation, the tumbling motion cannot occur in the DPPC planar bilayer due to the simulation setup. Nevertheless, we can discuss realistic τ_c of (essentially) planar membrane by substituting the computational $\rho(r)r^{-6}$ and the experimental σ to eq 14.[83]

Table 2 shows the τ_c values for the DPPC vesicles estimated by combining the NOE experimental σ in Figure 7 and the MD $\rho(r)r^{-6}$ in Figure 8. The $\rho(r)r^{-6}$ is assumed to be invariant

Table 2. Correlation Times in the DPPC Vesicles with a Varity of Diameters from the Combined NOE-MD Analysis[a]

	τ_c (ns)					
diameter (nm)	PCγ/PCβ	PCγ/PCα	PCγ/PCg2	PCγ/PC2	PCγ/PC3−15	PCγ/PC16
30[b]	0.29 (0.45)	0.15 (0.39)	0.31 (0.50)	1.9 (1.9)	6.5 (6.5)	8.4 (8.4)
50	1.0	0.82	1.7	7.9	44	75
100	1.4	1.1	2.1	6.8	55	110
200	1.1	0.82	2.1	10	55	130
400	1.1	0.90	1.7	10	54	160
800	1.0	1.0	2.1	14	63	170

[a] The data are shown in two digits. [b] τ_c value evaluated from eq 17 with single exponential is shown in parentheses. The disagreement betweeen the two τ_c values from eqs 14 and 17 for PCγ/PCβ, PCγ/PCα, and PCγ/PCg2 reflects the fact that $1/\omega_0 \ll \tau_c$ does not hold, where $1/\omega_0 = 0.27$ ns for the 600 MHz NMR apparatus presently employed.

against the curvature, and its value for the planar DPPC membrane is employed. This assumption is reasonable for PCγ/PCβ since $\rho(r)r^{-6}$ computed from the MD is different by only ∼20% between the PaLPC micelle and the DPPC planar bilayer. For PCγ/PC16, $\rho(r)r^{-6}$ differs by an order of magnitude. When the micelle value of $\rho(r)r^{-6}$ is used, the τ_c value reduces by a factor of ∼10 from the value in Table 2. In any case, the trend of the curvature dependence is not affected. In fact, $\rho(r)r^{-6}$ is expected to be larger at a larger curvature and the curvature dependence of τ_c will be stronger than that shown in Table 2 if the curvature dependence of $\rho(r)r^{-6}$ is taken into account.

According to Table 2, the time scale evidently varies between 30 nm (SUV) and 50 nm or more (LUV) in diameter. In the curvature range of LUV, the τ_c stays around 1 ns for PCγ/PCβ and increases gradually for distant sites. The dynamical inhomogeneity is more pronounced for a membrane with smaller curvature. The τ_c for PCγ/PC16 is in the submicrosecond range for the DPPC membranes. Previous MD and NMR studies showed that the submicrosecond scale corresponds to the lateral diffusion and tumbling motion and demonstrated that slow motions in the membrane contribute to NOE.[34,37,44,46,53] In particular, the τ_c of PCγ/PC16 in the essentially planar membrane with 800 nm diameter is shown to be 170 ns in Table 2, in excellent agreement with the characteristic time scale of slow motion identified by Gawrisch, Feller, and co-workers.[34,44] Tables 1 and 2 also show the discrepancy for the DPPC between the τ_c obtained from the computational $C(t)$ alone and the τ_c obtained from the combined, experimental σ, and computational $\rho(r)r^{-6}$. The discrepancy seen in Tables 1 and 2 is interpreted as the lateral diffusion and the tumbling motion making significant contributions to $C(t)$ for distant sites.

The strong site-dependence of the correlation time τ_c due to the slow dynamics results in the curvature dependence of the NOE cross relaxation rate constant σ. As discussed in this section, the separation between r and τ_c is problematic when multiple time scales of motion are involved, and MD simulation is powerful to dissect the contributions from r and τ_c. Actually, our scheme of NOE analysis relies only upon the statistical-mechanical expression for NOE cross relaxation rate constant and will be useful to treat other systems with slow motion such as transmembrane protein and ionic liquid.

4. CONCLUSIONS

The NOE cross intensity was studied in model-membrane systems over a wide range of curvatures with solution-state ^{1}H NMR-NOE and MD simulations. To suppress the broad components from the membrane signals and obtain the NOE intensities quantitatively, the conventional transient NOE method was combined with the spin−echo method (transient NOE-SE method). The broad components were found to be effectively suppressed by the spin−echo part, and an almost flat baseline was obtained. The transient NOE-SE method was confirmed to be valid with the SUV system of 30 nm in diameter through comparison to the conventional transient NOE method. The curvature dependence of the cross relaxation rate constant σ was observed from micelle to LUV of 800 nm in diameter. The NOE for micelle was detected only for the PCγ/PCβ pair and was too small for the other pairs with PCγ. The σ was then shown to increase with the diameter from SUV to LUV of ∼100 m and depend weakly on the diameter beyond ∼100 nm. For the LUVs, the σ was observed to be nonzero even for the most distant pair of PCγ/PC16. This observation does not imply the proximity of two terminal groups of PCγ and PC16, however. To reveal the origin of nonzero NOE for large vesicles, MD simulation was performed for PaLPC micelle and DPPC planar bilayer, and the distance distribution and the time correlation function were examined for PCγ/PCβ and PCγ/PC16. For PaLPC micelle, σ reflects mainly the distance information. For DPPC vesicle, in contrast, the correlation time τ_c was determined by the combination of the experimental σ and the computational distance distribution. It was found to depend on the proton pairs by orders of magnitude, showing a strong dynamical inhomogeneity for large vesicles.

About 1/3 of proteins stay in lipid membrane. Typically, the protein size is comparable to the size of lipid. In this case, the NOE might not be a valuable route to static structure since the correlation time determining the NOE would be strongly site-dependent. In turn, when combined with a method providing well-resolved spatial structure, such as MD and X-ray scattering, the NOE will be a valuable quantity to elucidate the dynamics. Therefore, the output of NOE measurement will be more dynamics-oriented than distance-oriented when the system of interest involves multiple orders of dynamical inhomogeneity. This is actually true not only for membrane systems but also for such emerging liquid systems as ionic liquid. Our analysis developed in the present work will be useful in revealing multiple time scales expected to be present in ionic liquids.

AUTHOR INFORMATION

Corresponding Author

*E-mail: nobuyuki@scl.kyoto-u.ac.jp.

■ ACKNOWLEDGMENT

This work is supported by Grants-in-Aid for Scientific Research (Nos. 21300111, 21850021, and 23651202) from the Japan Society for the Promotion of Science, and by a Grant-in-Aid for Scientific Research on Priority Areas (No. 20038034), a Grant-in-Aid for Scientific Research on Innovative Areas (No. 20118002), and the Next-Generation Supercomputing Project, Nanoscience Program from the Ministry of Education, Culture, Sports, Science, and Technology. N.M. is also grateful for the grants from the Association of the Progress of New Chemistry and the Suntory Institute of Bioorganic Research. K.Y. is grateful for the donations from the Takahashi Industrial and Economic Research Foundation, the Suzuki Foundation, and the Salt Science Research Foundation, No. 1114. Numerical calculations for the present work were carried out using the T2K Open Supercomputer at Center for Computational Sciences, University of Tsukuba.

■ REFERENCES

(1) Marrink, S. J.; Berendsen, H. J. C. *J. Phys. Chem.* **1996**, *100*, 16729–16738.
(2) Xiang, T. -X.; Anderson, B. D. *Biochim. Biophys. Acta* **1998**, *1370*, 64–76.
(3) Yau, W. -M.; Wimley, W. C.; Gawrisch, K.; White, S. H. *Biochemistry* **1998**, *37*, 14713–14718.
(4) Okamura, E; Nakahara, M. *J. Phys. Chem. B* **1999**, *103*, 3505–3509.
(5) Westh, P.; Trandum, C. *Biochim. Biophys. Acta* **1999**, 261–272.
(6) Banerjee, S.; Bennouna, M.; Ferreira-Marques, J.; Ruysschaert, J. M.; Caspers, J. *J. Colloid Interface Sci.* **1999**, *219*, 168–177.
(7) Wolfe, J.; Bryant, G. *Cryobiology* **1999**, *39*, 103–129.
(8) Okamura, E.; Kakitsubo, R.; Nakahara, M. *Langmuir* **1999**, *15*, 8332–8335.
(9) Zubrzycki, I. Z.; Xu, Y.; Madrid, M.; Tang, P. *J. Chem. Phys.* **2000**, *112*, 3437–3441.
(10) Gaede, H. C.; Gawrisch, K. *Biophys. J.* **2003**, *85*, 1734–1740.
(11) Mukhopadhyay, P; Vogel, H. J.; Tieleman, D. P. *Biophys. J.* **2004**, *86*, 337–345.
(12) Okamura, E.; Wakai, C.; Matubayasi, N.; Sugiura, Y.; Nakahara, M. *Phys. Rev. Lett.* **2004**, *93*, 248101.
(13) Erilov, D. A.; Bartucci, R.; Guzzi, R.; Shubin, A. A.; Maryasov, A. G.; Marsh, D.; Dzuba, S. A.; Sportelli, L. *J. Phys. Chem. B* **2005**, *109*, 12003–12013.
(14) Griepernau, B.; Leis, S.; Schneider, M. F.; Sikor, M.; Steppich, D.; Böckmann, R. A. *Biochim. Biophys. Acta* **2007**, *1768*, 2899–2913.
(15) Wu, G.; Mikhailovsky, A.; Khant, H. A.; Fu, C.; Chiu, W.; Zasadzinski, J. A. *J. Am. Chem. Soc.* **2008**, *130*, 8175–8177.
(16) Scheidt, H. A.; Huster, D. *Acta Pharmacol. Sin.* **2008**, *29*, 35–49.
(17) Simons, K.; Vaz, W. L. C. *Annu. Rev. Biophys. Biomol. Struct.* **2004**, *33*, 269–295.
(18) Giordani, C.; Wakai, C.; Yoshida, K.; Okamura, E.; Matubayasi, N.; Nakahara, M. *J. Phys. Chem. B* **2008**, *112*, 2622–2628.
(19) Lingwood, D.; Simons, K. *Science* **2010**, *327*, 46–50.
(20) Lentz, B. R.; Barenholz, Y.; Thompson, T. E. *Biochemistry* **1976**, *15*, 4521–4528.
(21) Gaber, B. P.; Peticolas, W. L. *Biochim. Biophys. Acta* **1977**, *465*, 260–274.
(22) Brumm, T.; Jorgensen, K.; Mouritsen, O, G.; Bayerl, T. M. *Biophys. J.* **1996**, *70*, 1373–1379.
(23) Lewis, R. N. A. H.; McElhaney, R. N. *The Structure of Biological Membranes*, 2nd ed.; Yeagle, P. L., Ed.; CRC Press, LLC: Boca Raton, FL, 2005; Chapter 2.
(24) Ahmed, S.; Wunder, S. L. *Langmuir* **2009**, *25*, 3682–3691.
(25) Okamura, E.; Wakai, C.; Matubayasi, N.; Nakahara, M. *Chem. Lett.* **1997**, 1061–1062.
(26) Huang, H.; Ball, J. M.; Billheimer, J. T.; Schroeder, F. *Biochem. J.* **1999**, *344*, 593–603.
(27) Bigay, J.; Gounon, P.; Robineau, S.; Antonny, B. *Nature* **2003**, *426*, 563–566.
(28) Chenal, A.; Vernier, G.; Savarin, P.; Bushmarina, N. A.; Geze, A.; Guillain, F.; Gillet, D.; Forge, V. *J. Mol. Biol.* **2005**, *349*, 890–905.
(29) Gallop, J. L.; Butler, P. J. G.; McMahon, H. T. *Nature* **2005**, *438*, 675–678.
(30) McMahon, H. T.; Gallop, J. L. *Nature* **2005**, *438*, 590–596.
(31) Pencer, J.; Jackson, A.; Kučerka, N.; Nieh, M. P.; Katsaras, J. *Eur. Biophys. J.* **2008**, *37*, 665–671.
(32) Opella, S. J.; Marassi, F. M.; Gesell, J. J.; Valente, A. P.; Kim, Y.; Oblatt-Montal, M.; Montal, M. *Nat. Struct. Biol.* **1999**, *6*, 374–379.
(33) Huster, D.; Gawrisch, K. *J. Am. Chem. Soc.* **1999**, *121*, 1992–1993.
(34) Yau, W. M.; Gawrisch, K. *J. Am. Chem. Soc.* **2000**, *122*, 3971–3972.
(35) Prompers, J. J.; Brüschweiler, R. *J. Am. Chem. Soc.* **2001**, *123*, 7305–7313.
(36) Gawrisch, K.; Eldho, N. V.; Polozov, I. V. *Chem. Phys. Lipids* **2002**, *116*, 135–151.
(37) Gawrisch, K. *The Structure of Biological Membranes*, 2nd ed.; Yeagle, P. L., Ed.; CRC Press, LLC: Boca Raton, FL, 2005; Chapter 4.
(38) Umegawa, Y; Matsumori, N.; Oishi, T.; Murata, M. *Biochemistry* **2008**, *47*, 13463–13469.
(39) Matsuoka, S.; Inoue, M. *Chem. Commun.* **2009**, 5664–5675.
(40) Da Costa, G.; Mouret, L; Chevance, C; Le Rumeur, E.; Bondon, A. *Eur. Biophys. J.* **2007**, *36*, 933–942.
(41) Torrey, H. C. *Phys. Rev.* **1953**, *92*, 962–969.
(42) Westlund, P.; Lyndenbell, R. *J. Magn. Reson.* **1987**, *72*, 522–531.
(43) Brüschweiler, R.; Roux, B.; Blackledge, M.; Griesinger, C.; Karplus, M.; Ernst, R. R. *J. Am. Chem. Soc.* **1992**, *114*, 2289–2302.
(44) Feller, S. E.; Huster, D.; Gawrisch, K. *J. Am. Chem. Soc.* **1999**, *121*, 8963–8964.
(45) Halle, B. *J. Chem. Phys.* **2003**, *119*, 12372–12385.
(46) Pitman, M. C.; Suits, F.; Gawrisch, K.; Feller, S. E. *J. Chem. Phys.* **2005**, *122*, 244715.
(47) Moreno, M.; Castiglione, F.; Mele, A.; Pasqui, C.; Raos, G. *J. Phys. Chem. B* **2008**, *112*, 7826–7836.
(48) Ma, D.; Liu, Z.; Li, L.; Tang, P.; Xu, Y. *Biochemistry* **2005**, *44*, 8790–800.
(49) Jarymowycz, V. A.; Stone, M. *J. Chem. Rev.* **2006**, *106*, 1624–1671.
(50) Cavanagh, J.; Fairbrother, W. J.; Palmer, A. G., III; Rance, M.; Skelton, N. J. *Protein NMR Spectroscopy: Principles and Practice*; Academic Press: New York, 2006.
(51) Sivanandam, V. N.; Cai, J.; Redfield, A. G.; Roberts, M. F. *J. Am. Chem. Soc.* **2009**, *131*, 3420–3421.
(52) Roberts, M. F.; Redfield, A. G. *J. Am. Chem. Soc.* **2004**, *126*, 13765–13777.
(53) Roberts, M. F.; Redfield, A. G.; Mohanty, U. *Biophys. J.* **2009**, *97*, 132–141.
(54) Pabst, G.; Kučerka, N.; Nieh, M. -P.; Rheinstädter, M. C.; Katsaras, J. *Chem. Phys. Lipids* **2010**, *163*, 460–479.
(55) Rheinstädter, M. C.; Ollinger, C.; Fragneto, G.; Demmel, F.; Salditt, T. *Phys. Rev. Lett.* **2004**, *93*, 108107.
(56) Komatsu, H.; Okada, S. *Biochim. Biophys. Acta* **1995**, 270–280.
(57) Subbarao, N. K.; MacDonald, R. I.; Takeshita, K.; MacDonald, R. C. *Biochim. Biophys. Acta* **1991**, *1063*, 147–154.
(58) MacDonald, R. C.; MacDonald, R. I.; Menco, B. Ph. M.; Takeshita, K.; Subbrao, N. K.; Hu, L. R. *Biochim. Biophys. Acta* **1991**, *1061*, 297–303.
(59) Kölchens, S.; Ramaswami, V.; Birgenheier, J.; Nett, L.; O'Brien, D. F. *Chem. Phys. Lipids* **1993**, *65*, 1–10.
(60) Nakahara, M.; Wakai, C. *Chem. Lett.* **1992**, *5*, 809–812.
(61) Stonehouse, J.; Adell, P.; Keeler, J.; Shaka, A. J. *J. Am. Chem. Soc.* **1994**, *116*, 6037–6038.

(62) Stott, K.; Keeler, J.; Van, Q. N.; Shaka, A. J. *J. Magn. Reson.* **1997**, *125*, 302–324.
(63) Price, W. S. *Concepts Magn. Reson.* **1998**, *10*, 197–237.
(64) Brüschweiler, R.; Wright, P. E. *Chem. Phys. Lett.* **1994**, *229*, 75–81.
(65) Brüschweiler, R.; Case, D. A. *Prog. Nucl. Magn. Reson. Spectrosc.* **1994**, *26*, 27–58.
(66) Hayashi, H.; Yamanaka, T.; Miyajima, M.; Imae, T. *Chem. Lett.* **1994**, 2407–2410.
(67) Foloppe, N.; MacKerell, A. D., Jr. *J. Comput. Chem.* **2000**, *21*, 86–104.
(68) Feller, S. E.; MacKerell, A. D., Jr. *J. Phys. Chem. B* **2000**, *104*, 7510–7515.
(69) Klauda, J. B.; Brooks, B. R.; MacKerell, A. D., Jr.; Venable, R. M.; Pastor, R. W. *J. Phys. Chem. B* **2005**, *109*, 5300–5311.
(70) Klauda, J. B.; Pastor, R. W.; Brooks, B. R. *J. Phys. Chem. B* **2005**, *109*, 15684–15686.
(71) Jorgensen, W. L.; Chandrasekhar, J.; Madura, J. D.; Impey, R. W.; Klein, M. L. *J. Chem. Phys.* **1983**, *79*, 926–935.
(72) Feller, S. E.; Zhang, Y.; Pastor, R. W.; Brooks, B. R. *J. Chem. Phys.* **1995**, *103*, 4613–4621.
(73) Martyna, G. J.; Tobias, D. J.; Klein, M. L. *J. Chem. Phys.* **1994**, *101*, 4177–4189.
(74) Nagle, J. F.; Tristram-Nagle, S. *Biochim. Biophys. Acta* **2000**, 159–195.
(75) Miyamoto, S.; Kollman, P. A. *J. Comput. Chem.* **1992**, *13*, 952–962.
(76) Swope, W. C.; Andersen, H. C.; Berens, P. H.; Wilson, K. R. *J. Chem. Phys.* **1982**, *76*, 637–649.
(77) Phillips, J. C.; Braun, R.; Wang, W.; Gumbart, J.; Tajkhorshid, E.; Villa, E.; Chipot, C.; Skeel, R. D.; Kale, L.; Schulten, K. *J. Comput. Chem.* **2005**, *26*, 1781–1802.
(78) A maximum seems to be present for the PCγ/PCβ at 100 nm. To clarfy this, a longer measurement (several hours to a day) needs to be done for the low S/N due to the spin−echo.
(79) Leonenko, Z. V.; Finot, E.; Ma, H.; Dahms, T. E. S.; Cramb, D. T. *Biophys. J.* **2004**, *86*, 3783–3793.
(80) To examine the relaxation through the paramagnetic oxygen molecule O_2, the transient NOE-SE experiment was also performed for the SUV and LUV of 400 nm prepared by substituting O_2 with N_2. The NOE enhancements were found not to be affected by the O_2 substitution, and the O_2 effect on NOE is negligible.
(81) The tumbling motion of a micelle is estimated as τ_c = 6.6 ns on the basis of the isotropic rotational diffusion of a hard sphere of 5 nm in diameter. The τ_c of the PaLPC micelle in Table 1 is smaller than this value, and reflects the intramicelle motion.
(82) The detection limit of an NOE signal is S/N = ∼5. With this S/N, the detection limit of σ is 0.02 for PCγ/PCβ and 0.01 for PCγ/PC16.
(83) The use of eq 14 is valid for the vesicles with diameters of 50 nm or more since $1/\omega_0 \ll \tau_c$. τ_c determined by eq 14 is coincident to that determined by eq 17 with a single exponential.